Hydrol. Earth Syst. Sci., 20, 4359–4373, 2016
www.hydrol-earth-syst-sci.net/20/4359/2016/
doi:10.5194/hess-20-4359-2016

Hydrology and Earth System Sciences
Open Access
EGU

Regionalization of monthly rainfall erosivity patterns in Switzerland

Simon Schmidt[1], **Christine Alewell**[1], **Panos Panagos**[2], **and Katrin Meusburger**[1]

[1]Environmental Geosciences, University of Basel, Bernoullistrasse 30, 4056 Basel, Switzerland
[2]European Commission, Joint Research Centre, Institute for Environment and Sustainability, Via E. Fermi 2749, 21027 Ispra, Italy

Correspondence to: Simon Schmidt (si.schmidt@unibas.ch)

Received: 3 May 2016 – Published in Hydrol. Earth Syst. Sci. Discuss.: 9 May 2016
Revised: 6 September 2016 – Accepted: 30 September 2016 – Published: 26 October 2016

Abstract. One major controlling factor of water erosion is rainfall erosivity, which is quantified as the product of total storm energy and a maximum 30 min intensity (I_{30}). Rainfall erosivity is often expressed as R-factor in soil erosion risk models like the Universal Soil Loss Equation (USLE) and its revised version (RUSLE). As rainfall erosivity is closely correlated with rainfall amount and intensity, the rainfall erosivity of Switzerland can be expected to have a regional characteristic and seasonal dynamic throughout the year. This intra-annual variability was mapped by a monthly modeling approach to assess simultaneously spatial and monthly patterns of rainfall erosivity. So far only national seasonal means and regional annual means exist for Switzerland. We used a network of 87 precipitation gauging stations with a 10 min temporal resolution to calculate long-term monthly mean R-factors. Stepwise generalized linear regression (GLM) and leave-one-out cross-validation (LOOCV) were used to select spatial covariates which explain the spatial and temporal patterns of the R-factor for each month across Switzerland. The monthly R-factor is mapped by summarizing the predicted R-factor of the regression equation and the corresponding residues of the regression, which are interpolated by ordinary kriging (regression–kriging). As spatial covariates, a variety of precipitation indicator data has been included such as snow depths, a combination product of hourly precipitation measurements and radar observations (CombiPrecip), daily Alpine precipitation (EURO4M-APGD), and monthly precipitation sums (RhiresM). Topographic parameters (elevation, slope) were also significant explanatory variables for single months. The comparison of the 12 monthly rainfall erosivity maps showed a distinct seasonality with the highest rainfall erosivity in summer (June, July, and August) influenced by intense rainfall events. Winter months have the lowest rainfall erosivity. A proportion of 62 % of the total annual rainfall erosivity is identified within four months only (June–September). The highest erosion risk can be expected in July, where not only rainfall erosivity but also erosivity density is high. In addition to the intra-annual temporal regime, a spatial variability of this seasonality was detectable between different regions of Switzerland. The assessment of the dynamic behavior of the R-factor is valuable for the identification of susceptible seasons and regions.

1 Introduction

Rainfall has direct impacts on soil mobilization by processes like rapid wetting or splash and runoff effects and is, therefore, one of the main driving forces of water erosion. The R-factor, as one of the five soil erosion risk factors (rainfall erosivity, soil erodibility, slope steepness and length, cover management, and support practices) of the Revised Universal Soil Loss Equation (RUSLE) (Renard et al., 1997; Foster et al., 2008) expresses the impact of rainfall on soils in the form of rainfall erosivity. The RUSLE is widely used for calculating soil loss, but each of the five factors also has an essential message on its own. For instance, besides being an important driving factor of soil erosion, the R-factor can also be used to draw conclusions about soil vulnerability, flood hazards, natural hazards, or probability of droughts (Panagos et al., 2015).

Soil erosion by water is a major environmental issue in Switzerland, which has been measured (Konz et al., 2012; Alewell et al., 2014), mapped (Mosimann, 1990; Prasuhn, 2011, 2012), and modeled (Gisler et al., 2011; Prasuhn et al., 2013) extensively. In Switzerland, since the 1950s, soil erosion by water has increased under arable land (Weisshaidinger and Leser, 2006) as well as in mountain grasslands (Meusburger and Alewell, 2008). Mosimann et al. (1991) assessed a quantity of up to 20 % of all cultivated land in Switzerland to be affected by soil erosion. The costs of soil erosion for Switzerland's arable land were estimated to be about CHF 53 million yr^{-1} (USD 55.2 million yr^{-1}; Ledermann, 2012). Increasing trends of water erosion are predicted for Switzerland under future climate change due to more frequent and heavy rainfall during winter (Fuhrer et al., 2006). Trends towards increasing rainfall erosivity are already observable in the months of May to October (Meusburger et al., 2012).

Previously published studies on rainfall erosivity in Switzerland focused on national seasonal means (Panagos et al., 2015) or regional annual means (Friedli, 2006; Gisler et al., 2011; Meusburger et al., 2012; Prasuhn et al., 2013). Since Switzerland has a high spatial climate variability (humid continental to oceanic climate; Köppen, 1936), seasonal and temporal variations of the weather are consequential. As such, these spatiotemporal climate variations can be expected to influence patterns in the rainfall erosivity. Spatial and temporal patterns of *R*-factors have not yet been established and mapped for Switzerland although Meusburger et al. (2012) already showed the presence of a strong seasonality of the rainfall erosivity for stations clustered at different elevation classes in Switzerland. So far the lack of significant spatial covariates impeded the mapping of intra-annual rainfall erosivity patterns. The availability of hourly radar rainfall observations for Switzerland (CombiPrecip data; Sideris et al., 2014) might offer a new possibility for the modeling of rainfall erosivity maps for individual months. These spatiotemporal patterns are decisive in combination with spatiotemporal patterns of vegetation cover in order to allow for an accurate soil erosion risk assessment and relevant for a monthly and seasonal management of agriculture practices and hazard controls. A rather static approach, which aggregates either regional or temporal *R*-factors such as those presented by Meusburger et al. (2012), is not suitable to model the dynamic soil erosion risk on a seasonal scale. Furthermore, the impact of precipitation on rainfall erosivity can be assessed by determining the monthly erosivity density.

Here, we aim to assess the spatiotemporal variability of rainfall erosivity in Switzerland by

i. extending the network of gauging stations from Meusburger et al. (2012);

ii. producing monthly *R*-factor maps based on high-resolution spatial covariates using a regression–kriging approach;

iii. evaluating the spatiotemporal patterns of the seasonal *R*-factor dynamics;

iv. determining the spatiotemporal erosivity density.

2 Material and methods

2.1 Rainfall erosivity (*R*-factor) calculation

The rainfall erosivity expressed as *R*-factor in RUSLE is the summation of the total storm energy (E) of an erosive rainfall event times its corresponding maximum intensity over a time span of 30 min (I_{30}) within a certain time period (Brown and Foster, 1987). We used the erosive rainfall event thresholds defined by Renard et al. (1997), which were modified by Meusburger et al. (2012). The unit rainfall energy (e_r) (MJ ha^{-1} mm^{-1}) for each time interval is expressed as the intensity of rainfall (i_r) (mm h^{-1}) during that time interval. It is calculated by Brown and Foster (1987) as

$$e_r = 0.29[1 - 0.72\exp(-0.05 i_r)]. \quad (1)$$

The erosive rainfall event erosivity (EI_{30}) (MJ mm ha^{-1} h^{-1}) is a product of the unit rainfall energy (e_r) (Eq. 1) and its maximum rainfall amount within a 30 min interval (according to Wischmeier and Smith, 1978):

$$EI_{30} = \left(\sum_{r=1}^{k} e_r v_r\right) I_{30}, \quad (2)$$

where v_r is the rainfall volume (mm) during a time unit r and I_{30} is the maximum rainfall intensity within 30 min of the event (mm h^{-1}).

The monthly rainfall erosivity (R_{mo}) (MJ mm ha^{-1} h^{-1} $month^{-1}$) is the mean of the accumulated event erosivity (EI_{30}) (Eq. 2) within a month:

$$R_{mo} = \frac{1}{n}\sum_{j=1}^{n}\sum_{k=1}^{m_j}(EI_{30})_k, \quad (3)$$

where n is the recorded number of years with the number of erosive events (m_j) within a certain month j. k is the index of a single event with its corresponding event erosivity.

The event rainfall erosivity was calculated for each station by applying the algorithm of Meusburger et al. (2012) (http://esdac.jrc.ec.europa.eu/themes/r-factor-switzerland-version-2012). The event rainfall erosivity was averaged by months to a long-term monthly mean *R*-factor (R_{mo}). Originally, the 30 min maximum rainfall rate (I_{30}) is obtained by breakpoint precipitation data, which is recorded in intervals of fixed rainfall rates instead of fixed time intervals (Wischmeier and Smith, 1978; Hollinger et al., 2002). As stations recording breakpoints are rare in Switzerland, we used records with a fixed time interval of 10 min. Using small time intervals better represents breakpoint data and records the intensity more realistic. Longer

intervals might underestimate rainfall intensity (Porto, 2016; Panagos et al., 2016a). For time intervals shorter than 15 min Porto (2016) reported an overestimation compared to the commonly used $(EI_{30})_{15}$ (15 min interval) and proposed a mean conversion factor of 0.97 for all investigated stations in southern Italy. This rather small deviation can mainly be explained by the fact that the maximum intensity of the 10 min record is upscaled to the whole 30 min increment. To avoid this bias our algorithm uses a 30 min moving average to identify the maximum I_{30} and as such resembles the original approach of Wischmeier and Smith (1978) to obtain the I_{30} from "successive increments of essentially uniform intensity" (Wischmeier and Smith, 1978). As we are working with the same 10 min measuring interval at all 87 stations, no conversion factor was applied to homogenize the data (cf. Agnese et al., 2006; Porto, 2016; Panagos et al., 2016a). Usually, snow, snowmelt, and rainfall on frozen soil are not assessed in the R-factor (Renard et al., 1997). Thus, a temperature threshold of 0 °C was set to obtain only rainfall and exclude snow water equivalents, which are subject to uncertainty in rainfall erosivity assessments (Leek and Olsen, 2000). Temperature data were measured simultaneous to precipitation (for 71 stations) or were directly derived (for 16 stations) from the closest stations (within a distance of less than 20 km) at similar elevation with an hourly resolution. We assumed only minor variation in temperature within that distance at a similar elevation level.

Besides neglecting snow, we did not consider rainfall as hail, which mainly occurs during summer in Switzerland (Nisi et al., 2016; Punge and Kunz, 2016). Although, Hurni (1978) investigated the impact of hail on rainfall erosivity for single plots in Switzerland and concluded that a water equivalent amount of hail exceeds the one of rainfall, hail erosivity has not yet been considered for this study.

2.2 Stations

We extended the gauging station network of Meusburger et al. (2012) (10 min measuring intervals) by 23 % from 71 to an updated dataset of 87 stations (Fig. 1) and upgraded stations by a longer time series if available.

The stations are well distributed and were subject to a quality control (Begert et al., 2005; Nogler, 2012). The additional 16 stations were previously investigated for rainfall erosivity by Nogler (2012). The mean density of one gauging station is 474.5 km^2. The average distance of one station to all others is 113.6 km by a minimum distance to the closest station of 13.2 km and a maximum distance of two stations by 324.6 km. A majority of 72 % of all stations (63) have recorded data of at least 22 years. The mean length of observations is 19.5 years and thus meet the proposed minimum timescale requirements for rainfall erosivity calculations of a 15-year measuring period (Foster et al., 2008).

2.3 Data and covariates

The high intra-annual variability of rainfall erosivity was already discussed in Meusburger et al. (2012), but not spatiotemporally mapped. The monthly erosivity mapping in a country with a high proportion of remote Alpine areas requests a variety of erosivity influencing covariates. High temporal information on snow cover and snow water equivalents, high spatiotemporal information on rainfall and high spatial information on topography are acquired as covariates (Table 1) for the monthly erosivity maps since rainfall erosivity is mainly controlled by precipitation and relief parameters (Meusburger et al., 2012; Panagos et al., 2015, 2016b). All spatial covariates have a much higher resolution (spatial and temporal) than datasets used in previous R-factor studies for Europe (Panagos et al., 2015, 2016a) and Switzerland (Meusburger et al., 2012), and therefore the R-factor mapping is feasible at a higher spatial and temporal precision.

The long-term snow depth (derived from mean monthly snow depth by MeteoSwiss) on a monthly resolution was used as an approximation for snow. The monthly point data of snow depth were regionalized by inverse distance weighting. Hourly Swiss CombiPrecip data (geostatistical combination of rain gauge measurements at 150 automatic stations and three C band radar observations; Sideris et al., 2014) were aggregated and averaged to a long-term monthly mean. Long-term mean daily precipitation per month was calculated based on the daily values of Alpine precipitation in EURO4M-APGD (Isotta et al., 2014). Averaging the monthly spatial precipitation of RhiresM (MeteoSwiss, 2013) over the years leads to long-term monthly mean precipitation sums. The variables elevation, slope, and aspect are retrieved from a 2 m digital terrain model (SwissAlti3D) for Switzerland.

2.4 Mapping the seasonal variability of rainfall erosivity in Switzerland

Hanel et al. (2016) and Angulo-Martínez and Beguería (2009) tested different interpolation methods for Czech Republic (Hanel et al., 2016) and the Ebro Basin in Spain (Angulo-Martínez and Beguería, 2009). Both studies could confirm that a combination of regression and residual kriging (regression–kriging) is among the most suitable methods to interpolate rainfall erosivity. We also used regression–kriging (Hengl et al., 2004, 2007; Hengl, 2007) to map the monthly variability of rainfall erosivity in Switzerland. The regression–kriging approach employed on the monthly mean rainfall erosivity for each of the 87 stations (R_{mo}). In a first step a generalized linear regression (GLM) (Gotway and Stroup, 1997) is used to establish a regression between R_{mo} and the high-resolution covariates. The GLM relates the rainfall erosivity (target variables) to the covariates (Table 1) and predicts rainfall erosivity at the same scale as covariates are available (Odeh et al., 1995; McBratney et

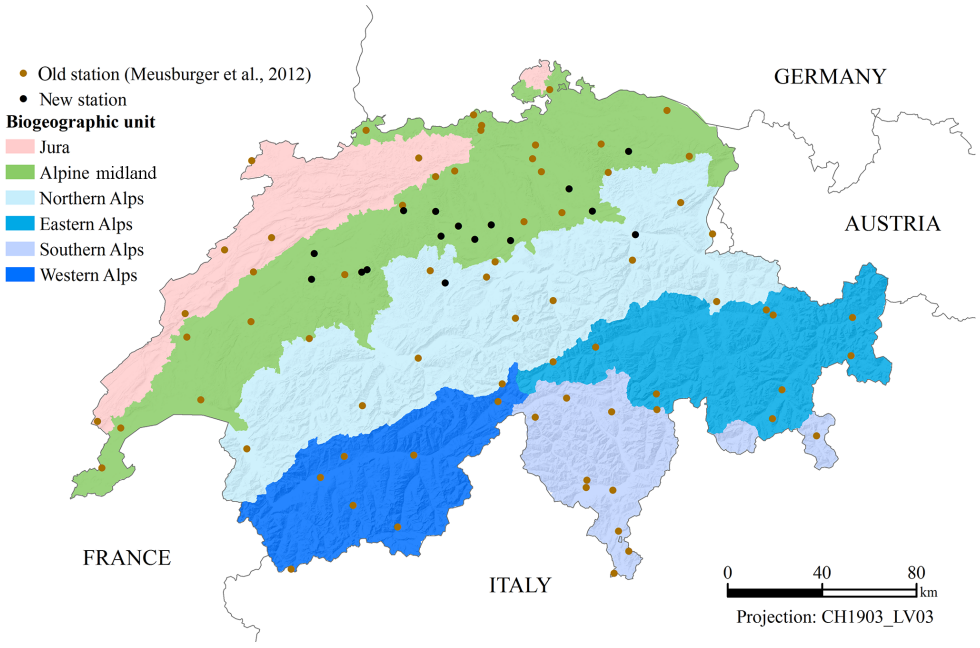

Figure 1. Biogeographic units and used gauging stations in Switzerland.

Table 1. Datasets used as covariates for the spatiotemporal mapping of rainfall erosivity.

Dataset	Derived information	Temporal resolution	Spatial resolution	Measuring period	Source	Information
Total snow depth	Long-term monthly snow depth	Hourly	58 stations	1988–2010	MeteoSwiss	–
CombiPrecip	Long-term monthly mean rainfall amount from measured and radar data	Hourly	1 km	2005–2015	MeteoSwiss	Sideris et al. (2014)
EURO4M-APGD	Long-term mean daily precipitation per month	Monthly	5 km	1971–2008	MeteoSwiss	Isotta et al. (2014)
RhiresM	Long-term mean monthly precipitation sums	Monthly	1 km	1961–2015	MeteoSwiss	MeteoSwiss (2013)
SwissAlti3D	Elevation, slope, aspect	–	2 m	–	SwissTopo	–

al., 2000). In an second step the residuals of the GLM are interpolated by an ordinary global kriging (McBratney et al., 2000; Hengl et al., 2004). Finally, the predicted rainfall erosivity by the GLM is summarized with the residuals map (established by the kriging procedure). The combination of interpolated R_{mo} with the spatial variation of its residuals enables the quantification of the standard error related to the erosivity mapping.

Besides the standard error maps, leave-one-out cross-validation (LOOCV) was used as a second quality check of the mapping procedure (Efron and Tibishirani, 1997). However, data splitting reduces the training observations and does not show the same results by repetition due to bias and randomness (Steyerberg, 2009; Harrell Jr., 2015). In contrast, LOOCV avoids a resampling bias since it omits only one observation from the dataset per run and estimates the model from the remaining $n-1$ observations. It yields the same regression coefficients by repetition due its reproducibility (James and Witten, 2015). In contrast, data split reduces the training observations and does not show the same coefficients due to randomness (Steyerberg, 2009; Harrell Jr., 2015). To compensate for the low validation subset, the process was repeated 100 times.

A log transformation of R_{mo} resulted in a normal distribution of the data. The suitability of each covariate for the GLM was determined by an automated stepwise feature selection process according to the Akaike information criterion (AIC). The α-to-enter significance level for covariate selection was set to 0.1 (Kutner et al., 2005; Gupta and Guttman, 2013). We also tested least absolute shrinkage and selection operator (LASSO) as an alternative feature selection method to the stepwise GLM, but it was less transparent for evaluation and showed inappropriate residual diagnostics (systematic error). Both, the LOOCV stepwise regression, as well

as LASSO, were performed in the *R*-package "caret" (v6.0-68). Outliers (Bonferroni-adjusted outlier test) and influential observations (Cook's distance) were omitted in the stepwise GLM.

The goodness-of-fit of the model was described by the coefficient of determination (R^2), the root mean square error (E_{RMS}), and the deviance. Regression diagnostics to evaluate the model included normality, non-constant error variance (homoscedasticity), multicollinearity (variance inflation factor, vif), and autocorrelation.

In all, 12 monthly maps of the long-term mean R_{mo} were derived by applying the regression equation with the covariates and their corresponding coefficients according to the individual monthly regression equation. The residuals of each months' stepwise GLM were interpolated by an ordinary global kriging with a stable variogram model and added to the R_{mo} maps in ESRI ArcGIS (v10.2.2.) afterwards.

Each monthly map is subject to an individual GLM. Therefore, a subset of individual covariates explains rainfall erosivity for each month separately. An averaging of 3-monthly maps leads to long-term seasonal mean *R*-factor (R_{seas}) maps for Switzerland with high spatial resolution. In addition, the sum of all 12 maps results in an updated (compared to Meusburger et al., 2012) long-term annual mean *R*-factor (R_{year}) map.

2.5 Cumulative daily *R*-factors

The averaged cumulative percentage of *R*-factor within a year is obtained and grouped by Swiss biogeographic regions (Gonseth et al., 2001). The biogeographic regions were selected because they show distinct differences in climate, soils, elevation, steepness, and geographic location. The cumulative curve of rainfall erosivity enables the extraction of the annual share of rainfall erosivity on a daily scale and is required for the calculation of RUSLE *C*-factors. *C*-factors are based on the product of the soil loss ratio (for a specific time of the year and a specific crop) and the cumulative percentage of rainfall erosivity of distinct days of the year (Wischmeier and Smith, 1978; Schwertmann et al., 1987; Renard et al., 1997). Therefore, all recorded rainfall events of a certain station within an individual biogeographic unit and at a specified day in the year are averaged over the measuring period and with the other stations of the region on a long-term mean daily level. That calculation of *C*-factors requires the percentage of the total annual rainfall erosivity of distinct days of the year, which can be derived by that procedure.

2.6 Monthly erosivity density

Monthly erosivity density (ED_{mo}) ($MJ\,ha^{-1}\,h^{-1}$) is calculated by the ratio of the long-term R_{mo} ($MJ\,mm\,ha^{-1}\,h^{-1}\,month^{-1}$) (neglecting snow) to mean monthly precipitation amount (P_{mo}) ($mm\,month^{-1}$) (including snow) according to the equation proposed by Foster et al. (2008):

$$ED_{mo} = \frac{R_{mo}}{P_{mo}}. \quad (4)$$

Small values (< 1) of ED_{mo} indicate that the influence of monthly precipitation on the monthly rainfall erosivity is mainly driven by its amount. On the other hand, high values of ED_{mo} show that relative to the absolute rainfall amount a high kinetic energy of rainfall was observed (e.g., strong storm events; Panagos et al., 2016b). The highest soil erosion risk is expected for areas where rainfall erosivity is high but related to a few intense rainfall events (high values of ED_{mo}). As such, ED_{mo} can reflect the temporal variability of rainfall intensity (Dabney et al., 2011) and can indicate how precipitation (short duration events with high intensities or high amounts of rainfall) controls the seasonality of rainfall. ED_{mo} was calculated using (i) the erosivity (R_{mo87}) and monthly precipitation sums (P_{mo87}) of each station (ED_{mo87}) and (ii) the 12 interpolated monthly rainfall erosivity maps R_{mo} and RhiresM as the monthly precipitation dataset (ED_{mo}). RhiresM is an already available precipitation dataset of MeteoSwiss that includes most of the 87 gauging stations. For the spatial mapping of monthly erosivity density, the interpolated monthly datasets R_{mo} and RhiresM were chosen since an interpolation of ED_{mo87} would require additional interpolation methods and spatial covariates, which are explanatory for the monthly erosivity density. Additionally, a performed interpolation might still modify the ED_{mo87} in accordance to the values at neighboring stations. According to Dabney et al. (2012), erosivity density is relatively independent of elevation up to a height of 3000 m a.s.l. In Switzerland, only the station Piz Corvatsch (COV) exceeds that threshold of height.

3 Results and discussion

3.1 Monthly rainfall erosivity at the 87 Swiss gauging stations

R_{mo} data averaged for all investigated stations show a bell-shaped curve over the 12 months (Fig. 2) with an increasing trend starting from February ($17.3\,MJ\,mm\,ha^{-1}\,h^{-1}\,month^{-1}$) to a maximum in July ($289\,MJ\,mm\,ha^{-1}\,h^{-1}\,month^{-1}$). The mean R_{mo} is $112\,MJ\,mm\,ha^{-1}\,h^{-1}\,month^{-1}$. The meteorological season winter (December–January–February) has the lowest mean R_{mo} ($33\,MJ\,mm\,ha^{-1}\,h^{-1}\,month^{-1}$), followed by spring (March–April–May; $68\,MJ\,mm\,ha^{-1}\,h^{-1}\,month^{-1}$), fall (September–October–November; $92\,MJ\,mm\,ha^{-1}\,h^{-1}\,month^{-1}$), and summer (June–July–August; $257\,MJ\,mm\,ha^{-1}\,h^{-1}\,month^{-1}$). Most of the monthly *R*-factors (96 %) of the lowest 10 % of all monthly values are part of the period between November and April, whereas 97 % of the highest 10 % are monthly rainfall erosivity in the period from May to October.

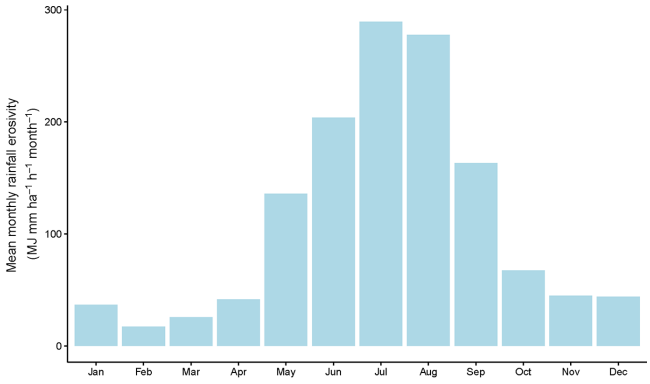

Figure 2. Mean monthly rainfall erosivity for all 87 Swiss stations.

The "Monthly Rainfall Erosivity" for Europe by Panagos et al. (2016a) and the national observations of Mosimann et al. (1990) for a single station in Switzerland (Bern, Swiss midland) comply with the present calculations with the highest rainfall erosivity for the season from June/July to August. The Swiss monthly rainfall erosivity in the European assessment (Panagos et al., 2016a) are on average by 3 MJ mm ha^{-1} h^{-1} month^{-1} smaller (after rescaling with the calibration factors from 30 to 10 min). That discrepancy by 5 % mainly arises due to the different numbers and time series of gauging stations.

Seasonality of R_{mo} on a continental scale is observed for Europe (Panagos et al., 2016a) and Africa (Vrieling et al., 2014), on a national scale for Brazil (da Silva, 2004), Cabo Verde (Mannaerts and Gabriels, 2000), Chile (Bonilla and Vidal, 2011), Denmark (Leek and Olsen, 2000), El Salvador (da Silva et al., 2011), Greece (Panagos et al., 2016b), Iran (Sadeghi et al., 2011; Sadeghi and Hazbavi, 2015; Sadeghi and Tavangar, 2015), Italy (Diodato, 2005; Borrelli et al., 2016), New Zealand (Klik et al., 2015), South Korea (Lee and Won, 2013), and inter alia for the regions of Australia (Yang et al., 2015; Yang and Yu, 2015), Belgium (Verstraeten et al., 2006), Brazil (da Silva et al., 2013), Cabo Verde (Sanchez-Moreno et al., 2014), China (Jing et al., 2009; Zhu et al., 2011; Wang et al., 2013; Zhao et al., 2015; Lai et al., 2016), England and Wales (Davison et al., 2005), Ethiopia (Meshesha et al., 2015), Japan (Laceby et al., 2016), the Himalayas (Ma et al., 2014), Italy (Terranova and Gariano, 2015), South Korea (Arnhold et al., 2014), Malaysia (Shamshad et al., 2008), Poland (Banasik and Górski, 1993; Banasik et al., 2001), Slovenia (Petkovšek and Mikoš, 2004; Mikoš et al., 2006), Spain (Renschler et al., 1999; Angulo-Martínez and Beguería, 2009), Turkey (Özşahin, 2014), and the USA (Wilkes and Sawada, 2005). However, the timing of the maximum and minimum erosivity varies considerably. Some of the above-mentioned studies show highest values in fall and winter (e.g., Greece), the highest values in March and the lowest values in July (e.g., Iran), or the highest values in January and the lowest values in July (e.g., Australia). The seasonal R_{mo} in Italy and Greece have lower ranges (209 and 121 MJ mm ha^{-1} h^{-1} month^{-1} compared to 272 MJ mm ha^{-1} h^{-1} month^{-1} in Switzerland), and the peak of the R-factor is shifted from July to September for Italy and to November for Greece.

3.2 Mapping of monthly rainfall erosivity and related uncertainties

All covariates – aspect excluded – were significant (p value < 0.1) within the stepwise regressions for at least 1 month to explain R_{mo} (Table 2). For each month, an individual selection of covariates was achieved by the stepwise GLM. The higher the ratio of the null deviance to the residual deviance, the better the model fits by including the covariates. The residual deviance is lower than the null deviance in all 12 investigated months. Monthly model efficiency and omitted influential outliers to increase the model's goodness of fit are summarized in Table 3. The monthly observations of R_{mo} at the 87 locations (exclusive outliers) as well as the residuals are normally distributed after the log transformation. A non-constant error (homoscedasticity), multicollinearity and non-autocorrelation were determined for all observations of the 12 months. H_0, which tests that all error variances are equal, was accepted by the Breusch–Pagan test in all cases and confirms homoscedasticity. Regression diagnostics further show a vif < 4 for each month. Therefore, we could not identify collinear data. According to a Durbin–Watson test, the Swiss R_{mo} dataset is not autocorrelated.

Model efficiency, averaged over all 12 months has a mean R^2 of 0.51 and a mean E_{RMS} of 93.27 MJ mm ha^{-1} h^{-1} month^{-1}. Among that period, R^2 varies between 0.10 (November) and 0.66 (July). E_{RMS} ranges from 6.98 to 330.16 MJ mm ha^{-1} h^{-1} month^{-1} within a year. Regression functions for November and December are most uncertain with the lowest R^2 and highest E_{RMS}. The low R^2 arise due to the generally low rainfall erosivity in winter that is mainly caused by lower rainfall amounts and higher amounts of snow (neglected in this study), which make it more challenging to predict R. The same constraint was observed in a study for Greece where the lowest R^2 was observed for the month with lowest rainfall erosivity (Panagos et al., 2016b). Even though, the spatial erosivity prediction for winter months is related to high uncertainties, the latter will have little effect on soil erosion assessment since rainfall erosivity has the lowest impact on soils in winter.

After adding the kriging interpolation of the residuals to the regionalization of monthly R-factors (based on the stepwise GLM), R^2 is increased in all months. As such, the regression–kriging improves the prediction of R-factors especially for months with low R^2 as in the case for November and December. The ranges of the stable variograms exceed the minimum distance (approx. 13.2 km) of neighboring stations in all months. The average prediction error of all

Table 2. Regression equations and selected covariates for estimating mean monthly rainfall erosivity in Switzerland.

Month	Regression equation
January	$R_{Jan} = 2.101 - 4.150 \cdot \text{CombiPrecip}_{Jan} - 0.006 \cdot \text{Snow depth}_{Jan} + 0.017 \cdot \text{Rhires}_{Jan} - 0.001 \cdot \text{Elevation}$
February	$R_{Feb} = 2.702 - 13.812 \cdot \text{CombiPrecip}_{Feb} - 0.007 \cdot \text{Snow depth}_{Feb} + 0.019 \cdot \text{Rhires}_{Feb} + 0.211 \cdot \text{Alpine Precip}_{Feb} - 0.001 \cdot \text{Elevation}$
March	$R_{Mar} = 2.534 - 7.735 \cdot \text{CombiPrecip}_{Mar} - 0.006 \cdot \text{Snow depth}_{Mar} + 0.018 \cdot \text{Rhires}_{Mar} + 0.170 \cdot \text{Alpine Precip}_{Mar} - 0.001 \cdot \text{Elevation}$
April	$R_{Apr} = 2.330 - 3.319 \cdot \text{CombiPrecip}_{Apr} - 0.008 \cdot \text{Snow depth}_{Apr} + 0.023 \cdot \text{Rhires}_{Apr} - 0.001 \cdot \text{Elevation} - 0.019 \cdot \text{Slope}$
May	$R_{May} = 2.965 + 2.072 \cdot \text{CombiPrecip}_{May} - 0.002 \cdot \text{Snow depth}_{May} + 0.015 \cdot \text{Rhires}_{May} - 0.001 \cdot \text{Elevation}$
June	$R_{Jun} = 3.890 + 0.014 \cdot \text{Rhires}_{Jun} - 0.001 \cdot \text{Elevation}$
July	$R_{Jul} = 3.926 + 5.710 \cdot \text{CombiPrecip}_{Jul} + 0.251 \cdot \text{Alpine Precip}_{Jul} - 0.001 \cdot \text{Elevation}$
August	$R_{Aug} = 3.627 + 0.010 \cdot \text{Rhires}_{Aug} + 0.194 \cdot \text{Alpine Precip}_{Aug} - 0.001 \cdot \text{Elevation}$
September	$R_{Sep} = 2.760 + 2.243 \cdot \text{CombiPrecip}_{Sep} + 0.539 \cdot \text{Alpine Precip}_{Sep} - 0.001 \cdot \text{Elevation}$
October	$R_{Oct} = 2.753 + 0.0161 \cdot \text{Rhires}_{Oct} - 0.001 \cdot \text{Elevation}$
November	$R_{Nov} = 2.665 + 3.787 \cdot \text{CombiPrecip}_{Nov} - 0.034 \cdot \text{Snow depth}_{Nov} + 0.166 \cdot \text{Alpine Precip}_{Nov}$
December	$R_{Dec} = 2.437 + 0.013 \cdot \text{Rhires}_{Dec}$ - 0.001 · Elevation

Table 3. Model efficiency by $R^2$and E_{RMS} as well as omitted outliers and influential observations per month.

Month	Excl. outlier stations	R^2	E_{RMS} (MJ mm ha^{-1} h^{-1} month^{-1})	Null deviance	Res. deviance
January	Mathod	0.52	6.98	70.36	20.65
February	Monte Generoso, Napf, Saetis	0.53	12.96	79.28	31.82
March	Col du Grand St-Bernard, Saetis	0.49	13.10	61.45	21.84
April	Col du Grand St-Bernard, Saetis, Weissfluhjoch	0.65	21.01	63.69	15.90
May	Davos, Col du Grand St-Bernard	0.60	73.39	56.28	16.83
June	Col du Grand St-Bernard	0.58	126.03	51.61	19.31
July	Monte Generoso, Col du Grand St-Bernard, Stabio	0.66	138.77	38.58	11.57
August	Col du Grand St-Bernard, Stabio	0.47	330.16	50.47	21.75
September	Col du Grand St-Bernard, Stabio	0.64	81.91	61.23	16.27
October	Piz Corvatsch, Col du Grand St-Bernard, Stabio	0.62	81.60	37.86	12.07
November	Piz Corvatsch, Col du Grand St-Bernard, Saetis	0.10	55.72	58.85	47.22
December	Col du Grand St-Bernard	0.26	177.65	73.90	50.66

12 months is −0.0055. The used stable semivariogram models are represented by 12 lag classes. Common patterns of increasing standard deviations with distances from gauging stations are recognizable in the standard deviation maps.

3.3 Monthly rainfall erosivity maps for Switzerland

Regionalized temporal patterns of modeled R_{mo} show a distinct seasonality with national means being the lowest in January (10.5 MJ mm ha^{-1} h^{-1} month^{-1}) and the highest in August (263.5 MJ mm ha^{-1} h^{-1} month^{-1}) (Table 4 and Fig. 3). Figure 3 represents R_{mo} on a stretch between 0 and 200 MJ mm ha^{-1} h^{-1} month^{-1} for a better spatial comparison of the color schemes although the R-factors are higher than 200 MJ mm ha^{-1} h^{-1} month^{-1} in summer (cf. Table 4). Winter is the season (Fig. 4) with the lowest rainfall erosivity. The highest R_{mo} peak in summer is consistent with the map of extreme point rainfall of 1 h duration (100-year return period; Spreafico and Weingartner, 2005), where the strong influence of extreme rainfall events on rainfall erosivity is indicated. Meusburger et al. (2012) already pointed to the relationship of thunderstorm activity to annual rainfall erosivity. The thunderstorm season in Switzerland lasts from late spring (May) to early fall (September). Thunderstorms are at least partly responsible for the high values of rainfall erosivity in summer. Starting from early fall (September), a decreasing trend of R_{mo} is noticeable all over Switzerland.

Averaged months are aggregated to representative seasons (R_{seas}) to identify spatial differences (Fig. 4). Spatially, mean winter rainfall erosivity show the highest values in the Jura Mountains, western and eastern parts of the northern Alps and the southern Alps (canton Ticino). High winter rainfall erosivity can be explained by rainfall resulting from low-pressure areas in northern Europe and weather fronts moved

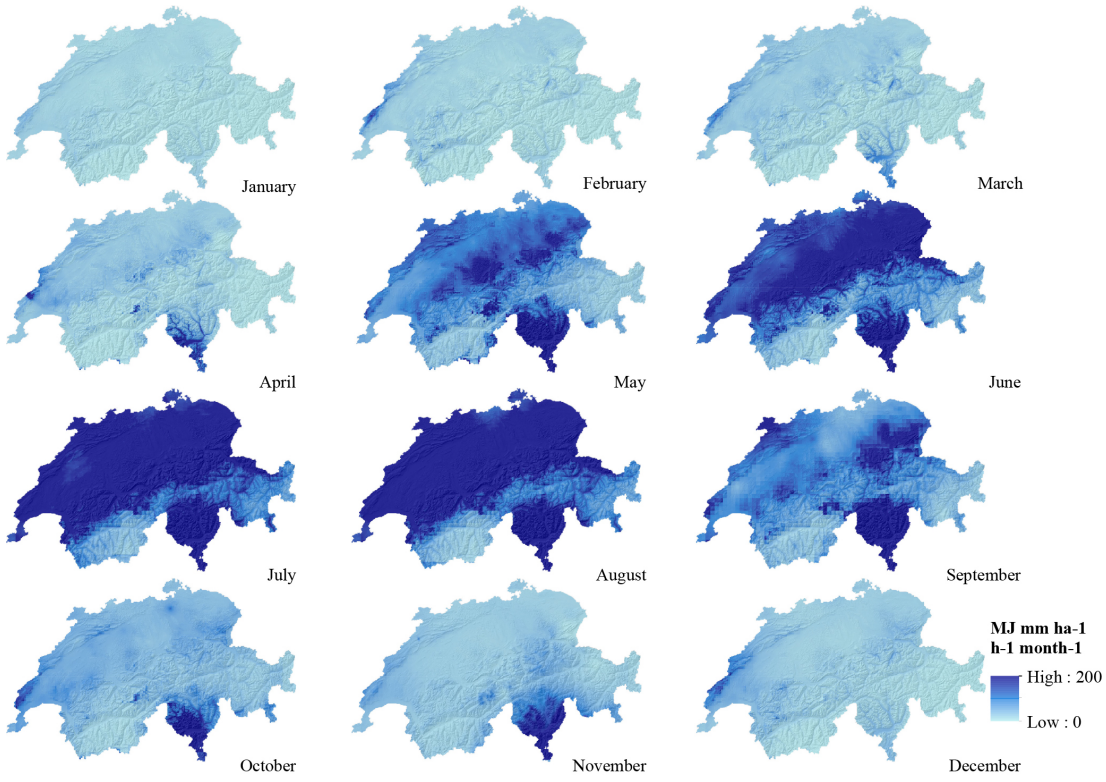

Figure 3. Monthly rainfall erosivity maps for Switzerland (equal stretch from 0 to 200 MJ mm ha^{-1} h^{-1} month^{-1}) derived by regression–kriging.

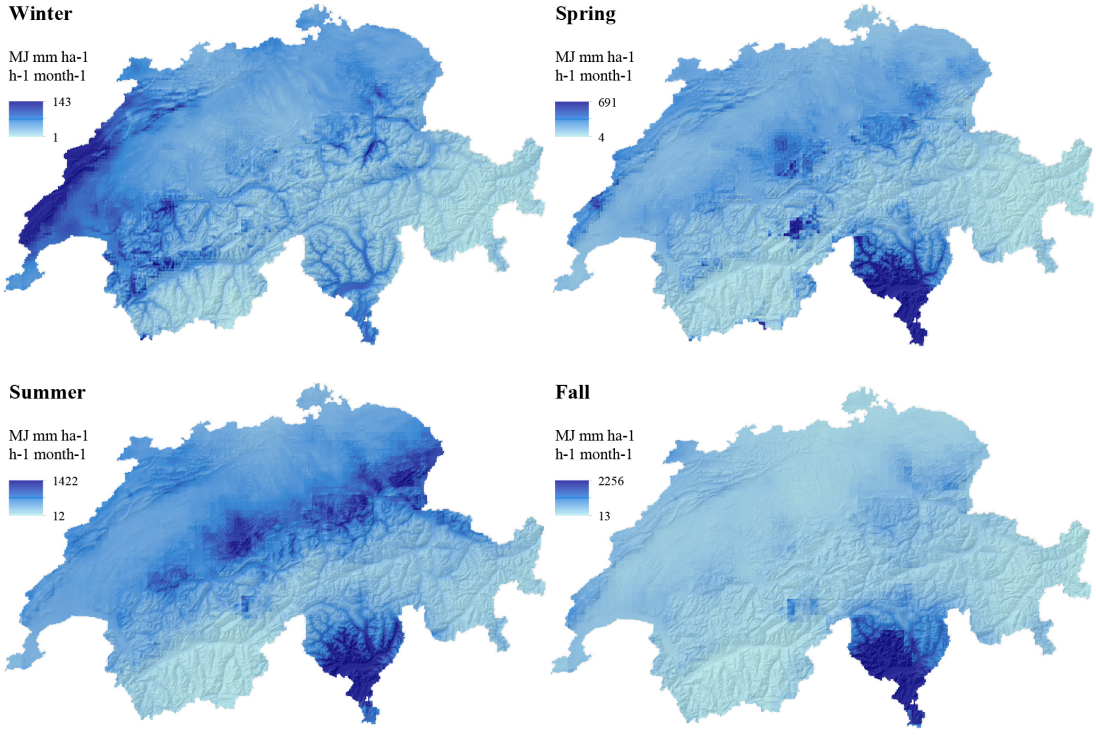

Figure 4. Seasonal rainfall erosivity maps for Switzerland derived by regression–kriging. The following months were averaged to derive seasonal maps: winter (December–February), spring (March–May), summer (June–August), fall (September–November).

Table 4. Monthly national rainfall erosivity in MJ mm ha^{-1} h^{-1} month^{-1}.

Month	Minima	Maxima	Mean
January	0.2	71.3	10.5
February	0.0	247.3	13.5
March	0.0	179.0	20.1
April	0.2	1014.4	28.8
May	8.3	1717.8	120.2
June	3.6	1262.1	174.8
July	12.6	1481.1	255.4
August	8.3	1994.9	263.5
September	6.8	6107.9	147.7
October	5.7	977.0	57.0
November	4.9	357.1	41.6
December	1.3	234.4	24.9

by northwesterly winds. These fronts are uplifted at the Jura Mountains which results in orographic rainfall. In spring, the northern and the southern Alps become more affected by high rainfall erosivity. The spatial variability of rainfall erosivity in spring in the southern Alps (canton Ticino) corresponds to the airflow from the south and the onset of the thunderstorm season in that region, which causes intense rainfall. High rainfall erosivity is persistent from spring to fall in the southern Alps. The generally high summer R-factors in the southern Alps, the Jura Mountains, and the northern Alpine foothill are driven by thunderstorms (van Delden, 2001; Perroud and Barder, 2013; Nisi et al., 2016; Punge and Kunz, 2016) and particularly in the southern Alps by high intense rainfall originating from orographic uplifts (Schwarb et al., 2001; Perroud and Barder, 2013). The cantons of Valais and Grisons remain with relatively low rainfall erosivity among all seasons due to lower convection and thereby lower rainfall erosivity in summer.

The degree of maximal variation at a certain location in a year (expressed as the difference between minimum and maximum monthly rainfall erosivity of all 12 months; Fig. 5) indicates the highest intra-annual range (up to 6086 MJ mm ha^{-1} h^{-1} month^{-1}) in the canton Ticino in the southern Alps. Furthermore, the northern Alps, Swiss midland, and Jura Mountains show a high erosivity variation within a year. The eastern and western Alps have the lowest ranges in accordance with their relatively low rainfall erosivity in a year. While the range map displays the absolute values of variation, the coefficient of variation map (ratio of standard deviation to the mean of all 12 months; Fig. S1 in the Supplement) indicates the relative degree of erosivity variation (in percent) at a certain location in a year. According to this map, the highest variation of up to 207 % can be observed in the eastern Alps (canton Grisons) were monthly rainfall erosivity is low and standard deviation is high. In the Muamba catchment in Brazil, high seasonal variations are also observed in regions with relatively low rainfall erosivity (da Silva et al., 2013).

Compared to the rainfall erosivity evaluation by Meusburger et al. (2012) on an annual scale, the observed mean R_{year} and spatial patterns only changed slightly due to the extended station network and higher resolution spatial covariates (aggregated by all 12 monthly R-factor maps). Improvements of the new map are the extended network of gauging stations, the cross-validation of the regression–kriging approach, and the inclusion of new high spatiotemporal covariates in order to increase the spatial resolution of the maps.

3.4 Cumulative daily rainfall erosivity

Generally, the steepest slopes of the cumulative rainfall erosivity curve for Switzerland can be noticed from June to September with a share of 62 % of the total annual rainfall erosivity within these 4 months (Fig. 6). That proportion complies with the cumulative sum of southwest Slovenia (63.2 %; Petkovšek and Mikoš, 2004) and exceeds the average share for Europe of 53 % (Panagos et al., 2016a) during the same period. A much larger proportion (90 %) of cumulative percentage of daily rainfall erosivity was observed for Bavaria (Schwertmann et al., 1987) and eastern Poland (78 %; Banasik and Górski, 1993). Mosimann et al. (1990) showed in a single-station approach (Bern, Swiss midland) that a proportion of 80 % of the total annual erosivity occurs in the period from April to September, which complies with the national share (resulting from the multi-station (87) calculation) of 77 % during the same period of a year.

All biogeographic units in Switzerland have similar trends of the cumulative daily rainfall erosivity. However, a Wilcoxon signed rank showed that all pairs of the sum curves of biogeographic regions have significant differences (significance level 0.05). The highest proportions (from June to September) and, therefore, steepest slopes can be identified for the southern Alps with a share of 70 % of the total sum. This high percentage of rainfall erosivity within a short period of time (4 months) is likely to have a large impact on the soil erosion susceptibility since it may coincide with the lowest (after harvesting of crops, carrots, etc.) and most unstable vegetation cover (after late sowing) (Hartwig and Ammon, 2002; Wellinger et al., 2006; Torriani et al., 2007; Prasuhn, 2011). Furthermore, fully grown pre-harvest field crops (e.g., cereals, maize) might suffer by bend over of corn stalks due to high intensity storms. In addition, water saturated conditions which are usual in May and September/October, make soils even more erodible. Highly susceptible soils in summer may also be expected in areas where forest fires occurred in spring and soils are uncovered by vegetation (which is the case especially for Ticino) (Marxer, 2003). The combination of the monthly rainfall erosivity maps with dynamic monthly C-factors might enable a monthly soil erosion risk assessment for Switzerland.

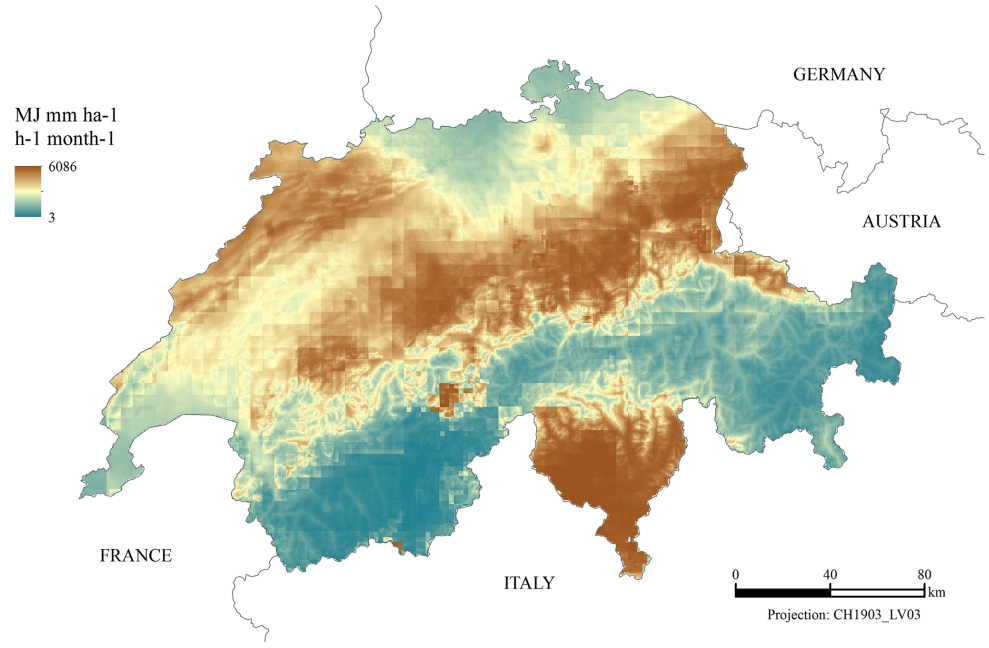

Figure 5. Range map (maximum R_{mo} minus minimum R_{mo}) for Switzerland showing the variability of rainfall erosivity in a year.

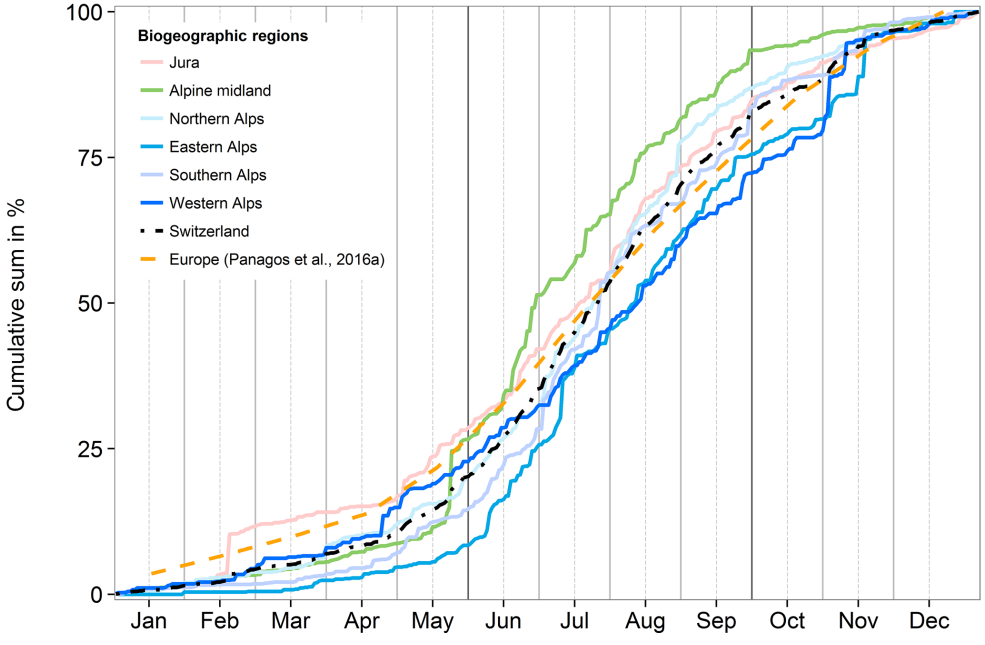

Figure 6. Cumulative daily rainfall erosivity proportion for Swiss biogeographic units, Switzerland and monthly rainfall erosivity for Europe (linear smoothed, European data from Panagos et al., 2016a).

3.5 Monthly erosivity density

Erosivity density (expressed as ratios of R to P) can be used to distinguish between high rainfall erosivity that is mainly influenced by high rainfall amounts and those that are influenced by relatively low rainfall amounts but highly intense rainfalls. That distinction helps to evaluate the potential consequences of rainfall erosivity for each month. The ED_{mo} maps (Fig. 7) show that the influence of rainfall intensity on rainfall erosivity also underlies seasonal and spatial variations.

Interpolated and spatially averaged ED_{mo} in winter is lower than $1\,MJ\,ha^{-1}\,h^{-1}$ (Fig. 7) for Switzerland. Therefore, rainfall intensity is not the driving factor for rainfall

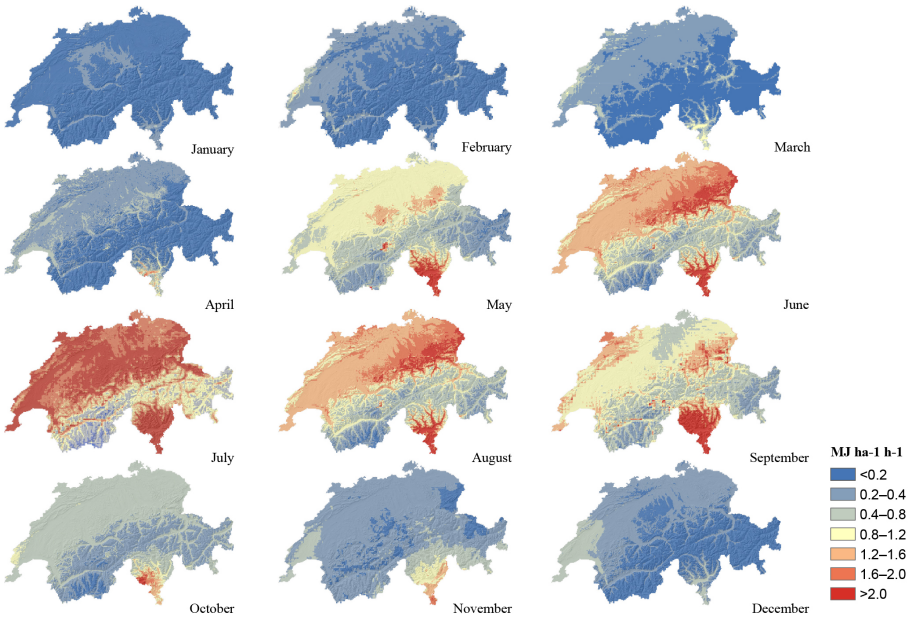

Figure 7. Monthly erosivity density (ED_{mo}) for Switzerland as ratio of monthly rainfall erosivity (R_{mo}) to monthly precipitation amount (P_{mo} based on RhiresM).

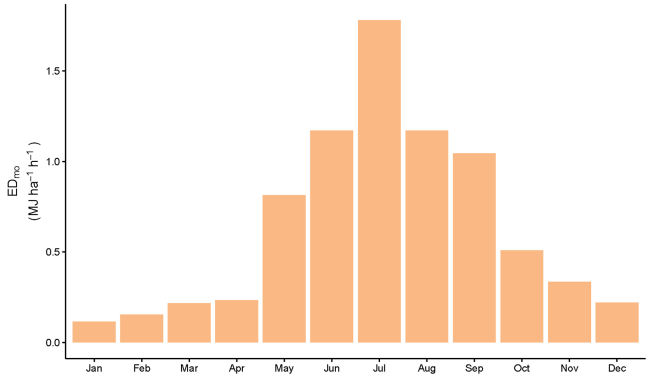

Figure 8. Mean monthly erosivity density (ED_{mo}) as ratios of R_{mo} (interpolated erosivity maps based on regression–kriging) to P_{mo} (precipitation sums from RhiresM) for Switzerland.

erosivity in these months, where low rainfall erosivity meets high rainfall amounts. The relatively high R_{mo} in the Jura Mountains is therefore mainly driven by large amounts of rainfall instead of high intensity rains. Interpolated and spatially averaged ED_{mo} has a maximum for Switzerland in July ($1.8\,MJ\,ha^{-1}\,h^{-1}$), which results from a relatively low rainfall amount indicating that rainfall erosivity is mainly controlled by high intensified events. Intense summer rainfall has its maximum in the regions of Jura, Swiss midland, northern Alpine foothill, and the southern Alps. In these regions, R_{mo} is high accompanied by relatively low precipitation amounts. As such, the erosivity risk is at its highest in the year, especially when soils are dry during periods of rare but high rainfall intensities and, therefore, infiltration is reduced due to crusts.

The distribution of the Swiss mean ED_{mo} (Fig. 8) is bell-shaped as is also the case for investigated stations in the USA, Italy, and Austria (Foster et al., 2008; Dabney et al., 2012; Borrelli et al., 2016; Panagos et al., 2016a). The monthly erosivity density of the neighboring country, Austria, complies with the Swiss values with minor variability. Greece, Italy, and the stations of the USA are characterized by higher ED_{mo} values than in Switzerland. Nonetheless, the conclusion Panagos et al. (2016b) drew for Greece is also generally valid for Switzerland; i.e., "rainfall erosivity is not solely dependent on the amount of precipitation".

In addition to the ED_{mo} maps, ED_{mo87} at the 87 stations (Table S1 in the Supplement) were calculated. ED_{mo87} show generally higher values than ED_{mo} calculated from the interpolated raster maps, since the interpolated R-factors are smoothed and adapted according to the surrounding values. This fact is also visible in Fig. S2 in the Supplement, where the relationship of absolute R-factors at the 87 stations (R_{mo87}) and the interpolated R-factors at the 87 stations (extracted after the interpolation with regression–kriging; $R_{regression–kriging}$) is presented.

4 Conclusion and outlook

The main aim of the current study was to investigate the seasonal and regional variability of rainfall erosivity in Switzerland. A crucial advancement of the present research was to identify spatial and temporal windows of high erosivity.

Through spatial–temporal mapping, it was possible to determine regions that are hardly affected by rainfall erosivity, such as Grisons and Wallis, and it was also possible to determine those that are only affected in a certain months, such as the Jura Mountains. The spatiotemporal variability of rainfall erosivity of Switzerland enables the controlled and time-dependent management of agriculture (like crop selection, time-dependent sowing) and droughts, ecosystem services evaluation, as well as for seasonal and regional hazard prediction (e.g., flood risk control, landslide susceptibility mapping). Rainfall erosivity based on high erosivity density has more severe impacts on soils, agriculture, droughts, and hazards in summer than in winter due the high impact of intense rainfalls.

In contrast to previous studies for Switzerland, which were either limited spatially (to a few stations) or temporally (to annual), we were able to produce 12 monthly spatiotemporal R-factor maps. The maps are based on high-resolution covariates in combination with an extended database of 87 automated gauging stations recording in 10 min intervals, showing simultaneously spatial and temporal variations of R-factors. Regression–kriging based on high-resolution covariates was a successful method for most of the months (mean $R^2 = 0.51$, $E_{\mathrm{RMS}} = 93.27\,\mathrm{MJ\,mm\,ha^{-1}\,h^{-1}\,month^{-1}}$). It was used to map the long-term monthly mean R-factors based on an extended database of rain-gauging stations. The spatiotemporal mapping of rainfall erosivity and erosivity density revealed that intense rainfall events in August trigger the highest national monthly mean rainfall erosivity value ($263.5\,\mathrm{MJ\,mm\,ha^{-1}\,h^{-1}\,month^{-1}}$). In particular the regions of Jura, Swiss midland, northern Alpine foothill, and Ticino in the southern Alps show pronounced rainfall erosivity during that month. The months June to September have a total share of 62 % of the total annual rainfall erosivity in Switzerland.

The current data highlight that rainfall erosivity has a very high variability within a year. These trends of seasonality vary between regions and consequently support that a dynamic soil erosion and natural hazard risk assessment is crucial. The combination of the temporally varying RUSLE factors (R- and C-factor) will lead to a more realistic and time-dependent estimation of soil erosion within a year, which is valuable for the identification of more susceptible seasons and regions. A mapping of the seasonality of the C-factor for a subsequent synthesis to a dynamic soil erosion risk assessment for Switzerland is envisaged in a later study.

The findings of this study have a number of important implications for soil conservation planning. Based on the knowledge of the variability of rainfall erosivity, agronomists can introduce selective erosion control measures, a change in crop or crop rotation to weaken of the rainfalls impact on soils and vegetation by increasing soil cover or stabilizing topsoil during these susceptible months. As such, a targeted erosion control for Switzerland not only reduces the direct costs of erosion by mitigation but also shrinks the costs for the implementation of control measures to a requested minimum.

5 Data availability

All commercial datasets of the present study were provided for scientific purpose within the framework of the research project N222-0350 funded by the Swiss Federal Office for the Environment (FEON). Precipitation and temperature data are obtained from MeteoSwiss (http://www.meteoswiss.ch; 71 stations) and the cantons Lucerne, Berne, and St. Gallen (16 stations). Total snow depth, CombiPrecip, EURO4M-APGD, and RhiresM were also provided by MeteoSwiss, SwissAlti3D from SwissTopo (http://www.swisstopo.ch).

The Supplement related to this article is available online at doi:10.5194/hess-20-4359-2016-supplement.

Author contributions. Simon Schmidt, Katrin Meusburger, and Christine Alewell analyzed the data, Simon Schmidt, Katrin Meusburger, Christine Alewell, and Panos Panagos wrote the paper.

Competing interests. The authors confirm and sign that there is no conflict of interest with networks, organizations, and data centers referred to in the paper.

Acknowledgements. The research has been funded by the Swiss Federal Office for the Environment (FOEN) (project no. N222-0350). The authors would like to thank O. G. Terranova, S.H. Sadeghi, and one anonymous referee for their valuable comments and suggestions to improve the quality of the paper. Furthermore the authors thank MeteoSwiss, SwissTopo, and the cantons Lucerne, Berne, and St. Gallen for providing the datasets.

Edited by: N. Ursino
Reviewed by: O. G. Terranova, S. H. Sadeghi, and one anonymous referee

References

Agnese, C., Bagarello, V., Corrao, C., D'Agostino, L., and D'Asaro, F.: Influence of the rainfall measurement interval on the erosivity determinations in the Mediterranean area, J. Hydrol., 329, 39–48, doi:10.1016/j.jhydrol.2006.02.002, 2006.

Alewell, C., Meusburger, K., Juretzko, G., Mabit, L., and Ketterer, M. E.: Suitability of 239+240 Pu and ^{137}Cs as tracers for soil erosion assessment in mountain grasslands, Chemosphere, 103, 274–280, doi:10.1016/j.chemosphere.2013.12.016, 2014.

Angulo-Martínez, M. and Beguería, S.: Estimating rainfall erosivity from daily precipitation records: A comparison among methods using data from the Ebro Basin (NE Spain), J. Hydrol., 379, 111–121, doi:10.1016/j.jhydrol.2009.09.051, 2009.

Arnhold, S., Lindner, S., Lee, B., Martin, E., Kettering, J., Nguyen, T. T., Koellner, T., Ok, Y. S., and Huwe, B.: Conventional and organic farming: Soil erosion and conservation potential for row crop cultivation, Geoderma, 219–220, 89–105, doi:10.1016/j.geoderma.2013.12.023, 2014.

Banasik, K. and Górski, D.: Evaluation of Rainfall Erosivity for East Poland, Proceedings of the Warsaw Symposium, 129–134, 1993.

Banasik, K., Górski, D., and Mitchell, J. K.: Rainall Erosivity for East and Central Poland, International Symposium on Soil Erosion Research for the 21st Century, 279–282, 2001.

Begert, M., Schlegel, T., and Kirchhofer, W.: Homogeneous temperature and precipitation series of Switzerland from 1864 to 2000, Int. J. Climatol., 25, 65–80, doi:10.1002/joc.1118, 2005.

Bonilla, C. and Vidal, K.: Rainfall erosivity in Central Chile, J. Hydrol., 410, 126–133, doi:10.1016/j.jhydrol.2011.09.022, 2011.

Borrelli, P., Diodato, N., and Panagos, P.: Rainfall erosivity in Italy: A national scale spatio-temporal assessment, Int. J. Dig. Earth, 1–16, 835–850, doi:10.1080/17538947.2016.1148203, 2016.

Brown, L. and Foster, G.: Storm Erosivity Using Idealized Intensity Distributions, T. ASAE, 30, 379–386, doi:10.13031/2013.31957, 1987.

da Silva, A. M.: Rainfall erosivity map for Brazil, CATENA, 57, 251–259, doi:10.1016/j.catena.2003.11.006, 2004.

da Silva, A. M., Wiecheteck, M., and Zuercher, B. W.: Spatial Assessment of Indices for Characterizing the Erosive Force of Rainfall in El Salvador Republic, Environ. Eng. Sci., 28, 309–316, doi:10.1089/ees.2010.0296, 2011.

da Silva, R. M., Santos, C. A. G., de Lima Silva, V. C., and Silva, L. P.: Erosivity, surface runoff, and soil erosion estimation using GIS-coupled runoff–erosion model in the Mamuaba catchment, Brazil, Environ. Monit. Assess., 185, 8977–8990, doi:10.1007/s10661-013-3228-x, 2013.

Dabney, S. M., Yoder, D. C., Vieira, D., and Bingner, R. L.: Enhancing RUSLE to include runoff-driven phenomena, Hydrol. Process., 25, 1373–1390, doi:10.1002/hyp.7897, 2011.

Dabney, S. M., Yoder, D. C., and Vieira, D. A. N.: The application of the Revised Universal Soil Loss Equation, Version 2, to evaluate the impacts of alternative climate change scenarios on runoff and sediment yield, J. Soil Water Conserv., 67, 343–353, doi:10.2489/jswc.67.5.343, 2012.

Davison, P., Hutchins, M. G., Anthony, S. G., Betson, M., Johnson, C., and Lord, E. I.: The relationship between potentially erosive storm energy and daily rainfall quantity in England and Wales, Sci. Total Environ., 344, 15–25, doi:10.1016/j.scitotenv.2005.02.002, 2005.

Diodato, N.: Predicting RUSLE (Revised Universal Soil Loss Equation) Monthly Erosivity Index from Readily Available Rainfall Data in Mediterranean Area, Environmentalist, 26, 63–70, doi:10.1007/s10669-006-5359-x, 2005.

Efron, B. and Tibshirani, R.: Improvements on Cross-Validation: The .632+ Bootstrap Method, J. Am. Stat. Assoc., 92, 548–560, doi:10.2307/2965703, 1997.

Foster, G. R., Yoder, D. C., Weesies, G. A., McCool, D. K., McGregor, K. C., and Bingner, R.: Draft User's Guide, Revised Universal Soil Loss Equation Version 2 (RUSLE-2), Washington, DC, 431 pp., 2008.

Friedli, S.: Digitale Bodenerosionsgefährdungskarte Der Schweiz Im Hektarraster – Unter Besonderer Berücksichtigung des Ackerlandes, Bern, 112 pp., 2006.

Fuhrer, J., Beniston, M., Fischlin, A., Frei, C., Goyette, S., Jasper, K., and Pfister, C.: Climate Risks and Their Impact on Agriculture and Forests in Switzerland, Clim. Change, 79, 79–102, doi:10.1007/s10584-006-9106-6, 2006.

Gisler, S., Lininger, H.-P., and Prasuhn, V.: Erosionsrisikokarte im 2×2-Meter-Raster (ERK2), Agrarforschung Schweiz, 2, 148–155, 2011.

Gonseth, Y., Wohlgemuth, T., Sansonnens, B., and Buttler, A.: Die biogeographischen Regionen der Schweiz. Erläuterungen und Einteilungsstandard, Umwelt Materialien Nr. 137 Bundesamt für Umwelt, Wald und Landschaft, Bern, 47 pp., 2001.

Gotway, C. A. and Stroup, W. W.: A Generalized Linear Model Approach to Spatial Data Analysis and Prediction, J. Agr. Biol. Environ. Stat., 2, 157–178, 1997.

Gupta, B. C. and Guttman, I.: Statistics and probability with applications for engineers and scientists, John Wiley & Sons Inc, Hoboken, New Jersey, 876 pp., 2013.

Hanel, M., Máca, P., Bašta, P., Vlnas, R., and Pech, P.: Rainfall erosivity factor in the Czech Republic and its Uncertainty, Hydrol. Earth Syst. Sci. Discuss., doi:10.5194/hess-2016-158, in review, 2016.

Harrell Jr., F.: Regression Modeling Strategies: With Applications to Linear Models, Logistic and Ordinal Regression, and Survival Analysis, Cham, http://www.springer.com/in/book/9783319194240, 582 pp., 2015.

Hartwig, N. L. and Ammon, H. U.: Cover crops and living mulches, Weed Sci., 50, 688–699, doi:10.1614/0043-1745(2002)050[0688:AIACCA]2.0.CO;2, 2002.

Hengl, T.: A practical guide to geostatistical mapping of environmental variables, EUR, 22904EN, Publications Office, Luxembourg, 290 pp., 2007.

Hengl, T., Heuvelink, G., and Rossiter, D.: About regression-kriging: From equations to case studies, Comp. Geosci., 33, 1301–1315, doi:10.1016/j.cageo.2007.05.001, 2007.

Hengl, T., Heuvelink, G., and Stein, A.: A generic framework for spatial prediction of soil variables based on regression-kriging, Geoderma, 120, 75–93, doi:10.1016/j.geoderma.2003.08.018, 2004.

Hollinger, S. E., Angel, J. R., and Palecki, M. A.: Spatial Distribution, Variation, an Trends in Storm Precipitation Characteristics Associated with Soil Erosion in the United States, Champaign, 90 pp., 2002.

Hurni, H.: Bestimmung der Erosivität von Hagelereignissen: Empirische Bestimmung der Erosivität von Hagelereignissen, unpublished manuscript, 1978.

Isotta, F., Frei, C., Weilguni, V., Perčec T., M., Lassègues, P., Rudolf, B., Pavan, V., Cacciamani, C., Antolini, G., Ratto, S., Munari, M., Micheletti, S., Bonati, V., Lussana, C., Ronchi, C., Panettieri, E., Marigo, G., and Vertačnik, G.: The climate of daily precipitation in the Alps: Development and analysis of a high-resolution grid dataset from pan-Alpine rain-gauge data, Int. J. Climatol., 34, 1657–1675, doi:10.1002/joc.3794, 2014.

James, G. and Witten, D.: An introduction to statistical learning: With applications in R, Corr. at 6. printing, Springer texts in statistics, Springer, New York, NY, 426 pp., 2015.

Jing, Z., Xu-dong, Z., Jin-xing, Z., Xiao-ling, Z., and Zhong-jian, W.: Calculation and Characterization of Rainfall Erosivity in Small Watersheds of Hilly Region in Northwest Hunan (in Chinese), J. Ecol. Rural Environ., 25, 32–36, 2009.

Klik, A., Haas, K., Dvorackova, A., and Fuller, I. C.: Spatial and temporal distribution of rainfall erosivity in New Zealand, Soil Res., 53, 815–825, doi:10.1071/SR14363, 2015.

Konz, N., Prasuhn, V., and Alewell, C.: On the measurement of alpine soil erosion, CATENA, 91, 63–71, doi:10.1016/j.catena.2011.09.010, 2012.

Köppen, W.: Das geographische System der Klimate, Handbuch der Klimatologie, 1, Berlin, 44 pp., 1936.

Kutner, M. H., Nachtsheim, C., Neter, J., and Li, W.: Applied linear statistical models, 5. ed., McGraw-Hill/Irwin series Operations and decision sciences, Boston, 1396 pp., 2005.

Laceby, J. P., Chartin, C., Evrard, O., Onda, Y., Garcia-Sanchez, L., and Cerdan, O.: Rainfall erosivity in catchments contaminated with fallout from the Fukushima Daiichi nuclear power plant accident, Hydrol. Earth Syst. Sci., 20, 2467–2482, doi:10.5194/hess-20-2467-2016, 2016.

Lai, C., Xiaohong, C., Zhaoli, W., Xushu, W., Shiwei, Z., Xiaoqing, W., and Wenkui, B.: Spatio-temporal variation in rainfall erosivity during 1960–2012 in the Pearl River Basin, China, CATENA, 137, 382–391, doi:10.1016/j.catena.2015.10.008, 2016.

Ledermann, T.: Multiple Implications of Soil Erosion and Conservation on Arable Farm Land in the Swiss Midlands, Bern, 167 pp., 2012.

Lee, J. S. and Won, J. Y.: Analysis of the Characteristic of Monthly Rainfall Erosivity in Korea with Derivation of Rainfall Energy Equation, Journal of Korean Society of Hazard Mitigation, 13, 177–184, doi:10.9798/KOSHAM.2013.13.3.177, 2013.

Leek, R. and Olsen, P.: Modelling climatic erosivity as a factor for soil erosion in Denmark: Changes and temporal trends, Soil Use Manage., 16, 61–65, doi:10.1111/j.1475-2743.2000.tb00175.x, 2000.

Ma, X., He, Y., Xu, J., van Noordwijk, M., and Lu, X.: Spatial and temporal variation in rainfall erosivity in a Himalayan watershed, CATENA, 121, 248–259, doi:10.1016/j.catena.2014.05.017, 2014.

Mannaerts, C. and Gabriels, D.: Rainfall erosivity in Cape Verde, Soil Till. Res., 55, 207–212, doi:10.1016/S0167-1987(00)00104-5, 2000.

Marxer, P.: Oberflächenabfluß und Bodenerosion auf Brandflächen des Kastanienwaldgürtels der Südschweiz mit einer Anleitung zur Bewertung der post-fire Erosionsanfälligkeit (BA EroKaBr), Physiogeographica, 33, Wepf in Komm, Basel, 2003.

McBratney, A. B., Odeh, I. O., Bishop, T. F., Dunbar, M. S., and Shatar, T. M.: An overview of pedometric techniques for use in soil survey, Geoderma, 97, 293–327, doi:10.1016/S0016-7061(00)00043-4, 2000.

Meshesha, D., Tsunekawa, A., Tsubo, M., Haregeweyn, N., and Adgo, E.: Evaluating spatial and temporal variations of rainfall erosivity, case of Central Rift Valley of Ethiopia, Theor. Appl. Climatol., 119, 515–522, doi:10.1007/s00704-014-1130-2, 2015.

MeteoSwiss: Documentation of MeteoSwiss Grid-Data Products: Monthly and Yearly Precipitation: RhiresM and RhiresY, Zürich, 4 pp., 2013.

Meusburger, K. and Alewell, C.: Impacts of anthropogenic and environmental factors on the occurrence of shallow landslides in an alpine catchment (Urseren Valley, Switzerland), Nat. Hazards Earth Syst. Sci., 8, 509–520, doi:10.5194/nhess-8-509-2008, 2008.

Meusburger, K., Steel, A., Panagos, P., Montanarella, L., and Alewell, C.: Spatial and temporal variability of rainfall erosivity factor for Switzerland, Hydrol. Earth Syst. Sci., 16, 167–177, doi:10.5194/hess-16-167-2012, 2012.

Mikoš, M., Jošt, D., and Petkovšek, G.: Rainfall and runoff erosivity in the alpine climate of north Slovenia: A comparison of different estimation methods, Hydrol. Sci. J., 51, 115–126, doi:10.1623/hysj.51.1.115, 2006.

Mosimann, T., Crole-Rees, A., Maillard, A., Neyroud, J.-A., Thöni, M., Musy, A., and Rohr, W.: Bodenerosion im Schweizerischen Mittelland: Ausmass und Gegenmassnahmen, Bericht 51 des Nationalen Forschungsprogrammes Nutzung des Bodens in der Schweiz, Liebefeld-Bern, 262 pp., 1990.

Mosimann, T., Maillard, A., Musy, A., Neyroud, J.-A., Rüttimann, M., and Weisskopf, P.: Erosionsbekämpfung in Ackerbaugebieten: Ein Leitfaden für die Bodenerhaltung, Themenbericht des Nationalen Forschungsprogrammes "Nutzung des Bodes in der Schweiz", 187 pp., 1991.

Nisi, L., Martius, O., Hering, A., Kunz, M., and Germann, U.: Spatial and temporal distribution of hailstorms in the Alpine region: A long-term, high resolution, radar-based analysis, Q. J. Roy. Meteorol. Soc., 142, 1590–1604, doi:10.1002/qj.2771, 2016.

Nogler, S.: Erosvität der Niederschläge im schweizerischen Mittelland, Bern, 183 pp., 2012.

Odeh, I., McBratney, A. B., and Chittleborough, D. J.: Further results on prediction of soil properties from terrain attributes: Heterotopic cokriging and regression-kriging, Geoderma, 67, 215–226, doi:10.1016/0016-7061(95)00007-B, 1995.

Özşahin, E.: An assessment of monthly rainfall erosivity model for Amik Plain (Hatay, S TURKEY), Photon, 177–193, 2014.

Panagos, P., Ballabio, C., Borrelli, P., Meusburger, K., Klik, A., Rousseva, S., Tadić, M., Michaelides, S., Hrabalíková, M., Olsen, P., Aalto, J., Lakatos, M., Rymszewicz, A., Dumitrescu, A., Beguería, S., and Alewell, C.: Rainfall erosivity in Europe, Sci. Total Environ., 511, 801–814, doi:10.1016/j.scitotenv.2015.01.008, 2015.

Panagos, P., Borrelli, P., Spinoni, J., Ballabio, C., Meusburger, K., Beguería, S., Klik, A., Michaelides, S., Petan, S., Hrabalíková, M., Olsen, P., Aalto, J., Lakatos, M., Rymszewicz, A., Dumitrescu, A., Perčec Tadić, M., Diodato, N., Kostalova, J., Rousseva, S., Banasik, K., and Alewell, C.: Monthly Rainfall Erosivity: Conversion Factors for Different Time Resolutions and Regional Assessments, Water, 8, 119, 1–18, doi:10.3390/w8040119, 2016a.

Panagos, P., Ballabio, C., Borrelli, P., and Meusburger, K.: Spatio-temporal analysis of rainfall erosivity and erosivity density in Greece, CATENA, 137, 161–172, doi:10.1016/j.catena.2015.09.015, 2016b.

Petkovšek, G. and Mikoš, M.: Estimating the R factor from daily rainfall data in the sub-Mediterranean climate of southwest Slovenia/Estimation du facteur R à partir de don-

nées journalières de pluie dans le climat sub-méditerranéen du Sud-Ouest de la Slovénie, Hydrol. Sci. J., 49, 869–877, doi:10.1623/hysj.49.5.869.55134, 2004.

Perroud, M. and Bader, S.: Klimaänderung in der Schweiz. Indikatoren zu Ursachen, Auswirkungen, Massnahmen, Umwelt-Zustand, 86 pp., 2013.

Porto, P.: Exploring the effect of different time resolutions to calculate the rainfall erosivity factor R in Calabria, southern Italy, Hydrol. Process., 30, 1551–1562, doi:10.1002/hyp.10737, 2016.

Prasuhn, V.: Soil erosion in the Swiss midlands: Results of a 10-year field survey, Geomorphology, 126, 32–41, doi:10.1016/j.geomorph.2010.10.023, 2011.

Prasuhn, V.: On-farm effects of tillage and crops on soil erosion measured over 10 years in Switzerland, Soil Tillage Res., 120, 137–146, doi:10.1016/j.still.2012.01.002, 2012.

Prasuhn, V., Liniger, H., Gisler, S., Herweg, K., Candinas, A., and Clément, J.-P.: A high-resolution soil erosion risk map of Switzerland as strategic policy support system, Land Use Policy, 32, 281–291, doi:10.1016/j.landusepol.2012.11.006, 2013.

Punge, H. J. and Kunz, M.: Hail observations and hailstorm characteristics in Europe: A review, Atmospheric Research, 176–177, 159–184, doi:10.1016/j.atmosres.2016.02.012, 2016.

Renard, K. G., Foster, G., Weesies, G., McCool, D. K., and Yoder, D. C.: Prediction Soil Erosion by Water: A Guide to Conservation Planning with the Revised Universal Soil Loss Equation (RUSLE), Agriculture handbook, 703, 384 pp., 1997.

Renschler, C. S., Mannaerts, C., and Diekkrüger, B.: Evaluating spatial and temporal variability in soil erosion risk – rainfall erosivity and soil loss ratios in Andalusia, Spain, CATENA, 34, 209–225, doi:10.1016/S0341-8162(98)00117-9, 1999.

Sadeghi, S., Moatamednia, M., and Behzadfar, M.: Spatial and Temporal Variations in the Rainfall Erosivity Factor in Iran, J. Agr. Sci. Tech., 13, 451–464, 2011.

Sadeghi, S. H. and Tavangar, S.: Development of stational models for estimation of rainfall erosivity factor in different timescales, Nat. Hazards, 77, 429–443, doi:10.1007/s11069-015-1608-y, 2015.

Sadeghi, S. H. R. and Hazbavi, Z.: Trend analysis of the rainfall erosivity index at different time scales in Iran, Nat. Hazards, 77, 383–404, doi:10.1007/s11069-015-1607-z, 2015.

Sanchez-Moreno, J. F., Mannaerts, C. M., and Jetten, V.: Rainfall erosivity mapping for Santiago Island, Cape Verde, Geoderma, 217–218, 74–82, doi:10.1016/j.geoderma.2013.10.026, 2014.

Schwarb, M., Daly, C., Frei, C., and Schär, C.: Mean Seasonal Precipitation throughout the European Alps 1971–1990, in: Hydrological Atlas of Switzerland, edited by: Wingartner, R., Bern, Sect. 2.6, 2001.

Schwertmann, U., Vogl, W., and Kainz, M.: Bodenerosion durch Wasser: Vorhersage des Abtrags und Bewertung von Gegenmaßnahmen, Stuttgart, 64 pp., 1987.

Shamshad, A., Azhari, M. N., Isa, M. H., Hussin, W. W., and Parida, B. P.: Development of an appropriate procedure for estimation of RUSLE EI30 index and preparation of erosivity maps for Pulau Penang in Peninsular Malaysia, CATENA, 72, 423–432, doi:10.1016/j.catena.2007.08.002, 2008.

Sideris, I., Gabella, M., and Germann, U.: The CombiPrecip experience: development and operation of a real-time radar-raingauge combination scheme in Switzerland, 2014 International Weather Radar and Hydrology Symposium, 2014.

Spreafico, M. and Weingartner, R.: Hydrologie der Schweiz: Ausgewählte Aspekte und Resultate, Berichte des BWG, Serie Wasser, 137 pp., 2005.

Steyerberg, E.: Clinical Prediction Models: A Practical Approach to Development, Validation, and Updating, New York, NY, 500 pp., 2009.

Terranova, O. G. and Gariano, S. L.: Regional investigation on seasonality of erosivity in the Mediterranean environment, Environ. Earth Sci., 73, 311–324, doi:10.1007/s12665-014-3426-z, 2015.

Torriani, D. S., Calanca, P., Schmid, S., Beniston, M., and Fuhrer, J.: Potential effects of changes in mean climate and climate variability on the yield of winter and spring crops in Switzerland, Clim. Res., 34, 59–69, doi:10.3354/cr034059, 2007.

van Delden, A.: The synoptic setting of thunderstorms in western Europe, Atmos. Res., 56, 89–110, doi:10.1016/S0169-8095(00)00092-2, 2001.

Verstraeten, G., Poesen, J., Demarée, G., and Salles, C.: Long-term (105 years) variability in rain erosivity as derived from 10-min rainfall depth data for Ukkel (Brussels, Belgium): Implications for assessing soil erosion rates, J. Geophys. Res., 111, 1–11, doi:10.1029/2006JD007169, 2006.

Vrieling, A., Hoedjes, J. C., and van der Velde, M.: Towards large-scale monitoring of soil erosion in Africa: Accounting for the dynamics of rainfall erosivity, Global Planet. Change, 115, 33–43, doi:10.1016/j.gloplacha.2014.01.009, 2014.

Wang, L. L., Yang, E., Huang, J., and Jiao, P.: Spatial and Temporal Characteristics of Rainfall Erosivity of Shanghai in Recent Ten Years, Appl. Mech. Mater., 295–298, 2084–2089, doi:10.4028/www.scientific.net/AMM.295-298.2084, 2013.

Weisshaidinger, R. and Leser, H.: Switzerland, in: Soil erosion in Europe, edited by: Boardman, J. and Poesen, J., Wiley-Interscience, Hoboken, NJ, 231–244, 2006.

Wellinger, R., Buser, H.-P., Krauss, J., and Theiler, R.: Karotten: Anbau, Erntezeitpunkt und Lagerung, Agrarforschung Schweiz, 13, 412–417, 2006.

Wilkes, G. and Sawada, M.: Geostatistically Derived Great Lakes USLE Monthly Rainfall Erosivity Factors, J. Great Lakes Res., 31, 155–165, doi:10.1016/S0380-1330(05)70247-1, 2005.

Wischmeier, W. H. and Smith, D. D.: Predicting rainfall erosion losses, Agriculture handbook, 537, US Gov. Print Off, Washington, 58 pp., 1978.

Yang, X. and Yu, B.: Modelling and mapping rainfall erosivity in New South Wales, Australia, Soil Res., 53, 178–189, doi:10.1071/SR14188, 2015.

Yang, X., Yu, B., and Zhu, Q.: Climate change impacts on rainfall erosivity and hillslope erosion in NSW, 21st International congress on Modelling and Simulation, Gold Coarst, Australia, 1572–1578, 2015.

Zhao, Q., Liu, Q., Ma, L., Ding, S., Xu, S., W., C., and Liu, P.: Spatiotemporal variations in rainfall erosivity during the period of 1960–2011 in Guangdong Province, southern China, Theor. Appl. Climatol., doi:10.1007/s00704-015-1694-5, 2015.

Zhu, Q., Chen, X., Fan, Q., Jin, H., and Li, J.: A new procedure to estimate the rainfall erosivity factor based on Tropical Rainfall Measuring Mission (TRMM) data, Sci. China Technol. Sci., 54, 2437–2445, doi:10.1007/s11431-011-4468-z, 2011.